Bridging Perception and Reasoning: Dual-Pipeline Neuro-Symbolic Landing for UAVs in Cluttered Environments

Weixian Qian*, Sebastian Schroder*, Yao Deng*,

Jiaohong Yao*, Linfeng Liang*, Xiao Cheng*, Richard Han*, and Xi Zheng*

*Macquarie University, Sydney, Australia

Abstract—Autonomous landing in unstructured (cluttered, uneven, and map-poor) environments is a core requirement for Unmanned Aerial Vehicles (UAVs), vet purely vision-based or deep learning models often falter under covariate shift and provide limited interpretability. We propose NEUROSYMLAND, a neurosymbolic framework that tightly couples two complementary pipelines: (i) an offline pipeline, where Large Language Models (LLMs) and human-in-the-loop refinement synthesize Scallop code from diverse landing scenarios, distilling generalizable and verifiable symbolic knowledge; and (ii) an online pipeline, where a compact foundation-based semantic segmentation model generates probabilistic Scallop facts that are composed into semantic scene graphs for real-time deductive reasoning. This design combines the perceptual strengths of lightweight foundation models with the interpretability and verifiability of symbolic reasoning. Node attributes (e.g., flatness, area) and edge relations (adjacency, containment, proximity) are computed with geometric routines rather than learned, avoiding the data dependence and latency of train-time graph builders. The resulting Scallop program encodes landing principles (avoid water and obstacles; prefer large, flat, accessible regions) and yields calibrated safety scores with ranked Regions of Interest (ROIs) and human-readable justifications. Extensive evaluations across datasets, diverse simulation maps, and real UAV hardware show that NEUROSYMLAND achieves higher accuracy, stronger robustness to covariate shift, and superior efficiency compared with state-of-the-art baselines, while advancing UAV safety and reliability in emergency response, surveillance, and delivery missions.

I. INTRODUCTION

Unmanned Aerial Vehicles (UAVs) increasingly operate near people and infrastructure, making safe landing the most safety-critical phase of a mission: a single misjudgment of terrain or bystanders can destroy the airframe and payload and endanger the surroundings. Despite steady progress in safelanding-zone (SLZ) detection, current markerless pipelines [1], [2], [3], [4] remain dominated by deep-learning methods that estimate SLZ feasibility from geometric cues (e.g., flatness, slope, roughness) and semantic cues (e.g., trees, people, vehicles). While effective at flagging unsafe regions, these models lack higher-level contextual semantics and compositional rules (e.g., " \forall construction zone \cap a crane \rightarrow unsafe" or " \forall place \in {school, station} \cap in operating hours \rightarrow unsafe"), limiting their ability to deliver verifiable, rule-based guarantees.

Moreover, SLZ objectives are inherently mission-dependent: emergency landings [5], [6] prioritize rapid risk reduction, rescue operations [7], [8], [9] weight proximity to casualties and access routes, while delivery missions [10], [11], [12] demand strict geofencing and bystander/property protections. Yet most pipelines remain scenario-agnostic, applying uniform

scoring and thresholds without reallocating the safety budget by task.

Prevailing SLZ methods are effectively black boxes [4], [13], [3], hindering certification, regression testing, and safety-case construction. Operators lack transparent, white-box justifications or formally checkable go/no-go gates [14].

To overcome these limitations, we present NEUROSYM-LAND —a neuro-symbolic SLZ selector that decouples perception from safety logic and is engineered for on-board efficiency. Rather than retraining perception, NEUROSYMLAND freezes a quantized foundation segmentation model (INT8) and concentrates adaptation on the symbolic layer. The pipeline operates in three tightly coupled stages: (i) a perception stage where the segmentation network with lightweight postprocessing (contour extraction, connected components, geometric moments, flatness/slope proxies, and short-horizon temporal smoothing) builds a probabilistic semantic scene graph with calibrated attributes and spatial relations; (ii) an offline rule-learning stage where an LLM [15], guided by human-inthe-loop edits over multiple landing sites and synthetic edge cases, synthesizes and validates safety rules that are compiled into probabilistic first-order logic (P-FOL) predicates; and (iii) an online inference stage where these rules are executed directly as a white-box safety gate over the scene graph, with mission-aware rule packs (emergency, rescue, delivery) producing auditable go/no-go decisions and enabling runtime updates without retraining the perception stack.

This design yields a data-efficient, interpretable, and verifiable SLZ decision process that outputs per-decision proof artifacts. In particular, NEUROSYMLAND delivers four key benefits: (1) provable guarantees within modeled assumptions, where candidate SLZs can be certified or refuted by solvers [16], [17]; (2) traceability and auditability, with replayable proof traces linked to safety requirements [18]; (3) customizability, since mission policies and geo-fences are encoded as editable logic rules [19]; and (4) continual updates without catastrophic forgetting, where new rules extend prior guarantees rather than overwrite them [20], [21]. By bridging foundation-model perception with interpretable symbolic reasoning, NEUROSYMLAND achieves SLZ detection that is efficient, testable, and certifiably safe, meeting both industrial and regulatory needs for UAV deployment.

In summary, this paper makes the following contributions:

 Offline neuro-symbolic pipeline. We introduce a rulesynthesis stage where an LLM, guided by human-in-theloop supervision, generates and iteratively refines Scallop code from limited flight scenarios. This process distills domain knowledge into verifiable symbolic rules that can be compiled into probabilistic first-order logic (P-FOL).

- Online neuro-symbolic pipeline. We pair an INT8quantized foundation segmentation model with lightweight geometric post-processing to construct a probabilistic, symbolic scene graph. The pre-validated rules execute directly as a white-box safety gate over this graph, producing auditable go/no-go decisions and enabling task reconfiguration (emergency, rescue, delivery) without retraining the perception stack.
- Experimental evaluation. Through software-in-the-loop (SIL) and hardware-in-the-loop (HIL) studies, we show that NEUROSYMLAND consistently outperforms both marker-based and markerless baselines in SLZ quality, robustness to dynamic agents, and interpretability. The system runs edge-ready in real time under tight compute and memory budgets, with no back-propagation at runtime, while providing per-decision proof traces for auditability.

The paper is organized as follows: Section II reviews related work, Section III presents our methodology, Section IV-A report the setup and results, and Section V concludes and outlines future directions.

II. RELATED WORK

A. UAV Safe Landing Zone Detection

Safe landing zone (SLZ) detection has historically included both marker-based and markerless approaches. Marker-based pipelines, which rely on fiducials such as AprilTag [22], [23] or ArUco [24], are increasingly impractical for industry use because they require costly deployment and maintenance of markers and remain brittle under glare, occlusion, or adverse weather. By contrast, markerless SLZ detection—now the industry's actual business requirement—is far more challenging, as it must infer safe terrain directly from onboard perception without any pre-installed infrastructure. Existing markerless pipelines estimate SLZ feasibility by combining geometric cues (flatness, slope, roughness, clearance) with semantic cues (people, vehicles, water) [1], [2], [3], [4]. While these methods show promising real-time performance on lightweight platforms, their definitions of safety remain relatively simple, often limited to low-level geometric thresholds or basic semantic vetoes, lacking contextual safety semantics, compositional rules, and formal verifiability.

B. Neuro-Symbolic Reasoning and LLM-Symbolic Integration

Neuro-symbolic (NeSy) approaches combine subsymbolic perception with symbolic reasoning to achieve systems that are data-driven yet interpretable and verifiable. Two strands are most relevant here: (i) neuro-symbolic models that expose deductive or probabilistic proof procedures, and (ii) LLM-driven symbolic reasoning, where large language models propose programs or constraints that are executed by formal solvers.

Neuro-symbolic models. Logic programming (e.g., Prolog [25]) established goal-directed, explainable proving.

This foundation has been extended to probabilistic reasoning (ProbLog [26]), neural–symbolic integration (Deep-ProbLog [27]), and differentiable inference (TensorLog [28]). Scallop [29] further advances this space by supporting discrete, probabilistic, and differentiable reasoning with provenance semantics at GPU scale, making it attractive for structured, verifiable decision-making.

LLM-driven symbolic reasoning. Recent work uses LLMs to synthesize executable programs or constraints for downstream solvers. Robotics examples include SayCan [30] and Code-as-Policies [31], while QA methods such as PAL [32] and SatLM [33] show the benefits of combining LLM generation with interpreters or SAT solvers for faithful logical reasoning. However, these methods have not been applied to safety-rule induction in UAV landing.

We close this gap by, for the first time, synthesizing Scallop code for UAV safe-landing-zone detection. Offline, we use an LLM with human-in-the-loop refinement to generate and validate safety rules, compiling them into verifiable Scallop programs. Online, we combine a quantized foundation segmentation model with lightweight geometric post-processing to build probabilistic scene graphs, where the Scallop rules execute as a white-box safety gate. This integration yields interpretable, auditable, and mission-conditioned SLZ decisions that are efficient, verifiable, and edge-ready.

III. METHODOLOGY

Our neuro-symbolic architecture, NEUROSYMLAND, couples offline rule learning (right) with online inference (left) to integrate foundation-model perception and Scallop-based reasoning (Fig. 1). The pipeline proceeds in three stages: First, a frozen, INT8-quantized semantic-segmentation backbone with lightweight post-processing lifts pixels into a probabilistic semantic scene graph; Second, an offline LLM+expert loop synthesizes and validates safety rules, compiled into Scallop probabilistic first-order logic (P-FOL); Third, at online inference, these rules execute as a white-box, mission-aware safety gate, where a selector applies task-specific rule packs (emergency, rescue, delivery) to yield auditable go/no-go decisions with minimal-witness explanations—without retraining perception.

A. Perception Backbone & Lightweight Post-processing

Our target platform is an edge device (Jetson Orin Nano Super, 8 GB) with tight power/thermal and memory budgets. Many prior *markerless* SOTA [4], [3], [2] pipelines rely on large backbones and multi-branch geometry heads (depth/BEV/MVS), which are impractical under these constraints. To keep the online inference system responsive while preserving accuracy, we deploy an INT8-quantized SegFormer-B0 [34] (fine-tuned on the Semantic Drone Dataset [35]) and apply lightweight OpenCV routines: thresholding (to binarize class posteriors), contour detection and connected components (to isolate candidate regions), polygon simplification (to reduce contour complexity), geometric moments (to compute centroid, orientation, compactness),

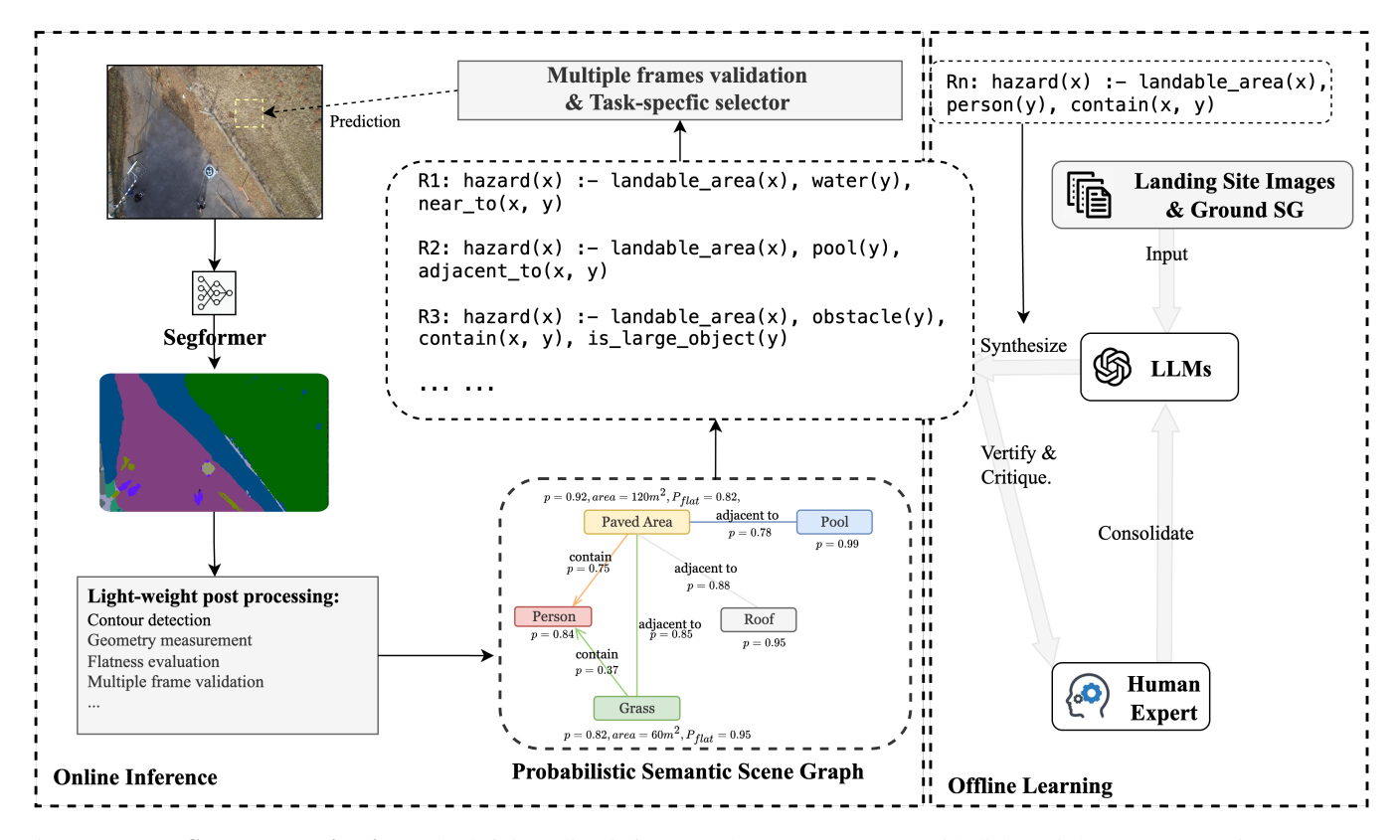


Fig. 1: **NEUROSYMLAND pipeline.** The left is online inference phase: SegFormer with lightweight post-processing (contours, distances, flatness/flow) extracts candidate regions. Cues are lifted to a probabilistic semantic scene graph; a Scallop-based, task-weighted selector infers hazards and ranks SLZs. Right: offline human-in-the-loop produces frozen rules for deployment.

flatness/slope proxies (from local geometry), and short-horizon temporal validation (to stabilize attributes across frames) [36] to extract and stabilize candidate regions. The resulting regions and their calibrated attributes are lifted into a probabilistic semantic scene graph whose nodes carry calibrated attributes (class probs/entropy, area, centroid, orientation, compactness, flatness, slope) and whose edges encode spatial relations (adjacency/touch, containment, center distance, proximity to hazards), yielding region-level evidence for the probabilistic scene graph components.

TABLE I: Probabilistic Scene Graph Components, aligned with the Semantic Drone Dataset [35]

Semantic Objects	unlabeled, paved-area, dirt, grass, gravel, water, rocks, pool, roof, wall, window, door, fence, person, dog, car, bicycle, tree, obstacle
Attributes	is_large_area, is_regular_shape, is_flat_surface, is_stable_surface, is_moving, is_smooth_surface, is_accessible, is_safe
Relations	above, bottom, left, right, adjacent_to, contain, on, near_to, far_from, surrounded_by

B. Probabilistic Semantic Scene Graph (PSSG)

As shown in Table I, we instantiate a Probabilistic Semantic Scene Graph (PSSG): G=(V,E), where nodes $v\in V$ are connected-component regions labeled by semantic objects (e.g., paved-area, grass, roof, person, car), and edges $e=(v,u)\in E$ encode Relations (e.g., adjacent_to, contain, on, near_to, surrounded_by). Each node carries a calibrated attribute vector a(v) over the Attributes set (e.g., is_flat_surface, is_stable_surface, is_moving), obtained by aggregating segmentation posteriors, geometric moments (area, centroid, orientation, compactness), flatness/slope proxies, and temporal smoothing across K frames. We represent evidence as probabilistic unary or binary predicates (e.g., paved_area(v)[p], is_flat_surface(v)[p], near_to(u,v)[p]). This factorization lifts pixels to region-level, uncertainty-aware facts that scale with |V| and |E| rather than image resolution.

C. Offline Learning: LLM-Human-in-the-Loop Scallop Code Synthesis

We depart from conventional supervised training and instead learn explicit Scallop [29] rules for UAV safe-landing-zone (SLZ) detection via an LLM-driven, expert-in-the-loop process. The key idea is to treat rule induction as a synthesis and verification loop rather than fitting a black-box model.

TABLE II: Representative Scallop rule examples for the safety gate.

ID	Scallop rule (Datalog style)	Intuition
R1	<pre>landable_area(x) :- (paved_area(x) V dirt(x) V grass(x)).</pre>	Paved, dirt, and grass are candidate landing surfaces.
R2	$\label{eq:human_related} \begin{array}{ll} \text{human_related(y) :- (person(y) V dog(y) V bicycle(y) V} \\ \text{car(y)).} \end{array}$	Group human-adjacent hazards.
R3	hazard(x) :- landable_area(x), water(y), near_to(x, y).	Water nearby is risky.
R4	$hazard(x) := landable_area(x), tree(y), near_to(x, y).$	Large trees near the touchdown are risky.
R5	<pre>hazard(x) :- landable_area(x), pool(y), adjacent_to(x, y).</pre>	Pools adjacent to a candidate are unsafe.
R6	$\label{eq:hazard(x):-landable_area(x), rocks(y), contain(x, y),} is_large_object(y).$	Large rocks inside the zone are unsafe.
R7	$\label{eq:hazard(x):-landable_area(x), vegetation(y), contain(x, y),} is_large_object(y).$	Dense vegetation in-zone is unsafe.
R8	$\label{eq:hazard(x):-landable_area(x), obstacle(y), contain(x, y),} is_large_object(y).$	Generic large obstacle in-zone is unsafe.
R9	<pre>hazard(x) :- paved_area(x), car(y), contain(x, y).</pre>	Vehicles occupying a paved zone are unsafe.
R10	$\label{eq:hazard} \texttt{hazard}(\texttt{x}) \; : - \; \texttt{paved_area}(\texttt{x}) , \; \texttt{human_related}(\texttt{y}) , \; \texttt{contain}(\texttt{x}, \; \texttt{y}) .$	People/dogs/bicycles/cars in a paved zone are unsafe.
R11	<pre>hazard(x) :- landable_area(x), building(y), adjacent_to(x, y).</pre>	Building right next to zone is risky.
R12	$\label{eq:hazard} \begin{array}{ll} \text{hazard}(x) : - \text{landable_area}(x) , & (\text{area_too_small}(x) \forall \\ \text{rough_surface}(x)) . \end{array}$	Insufficient touchdown/uneven area.
R13	<pre>safe(x) :- landable_area(x), not hazard(x).</pre>	A site is safe if landable and no hazard fires.

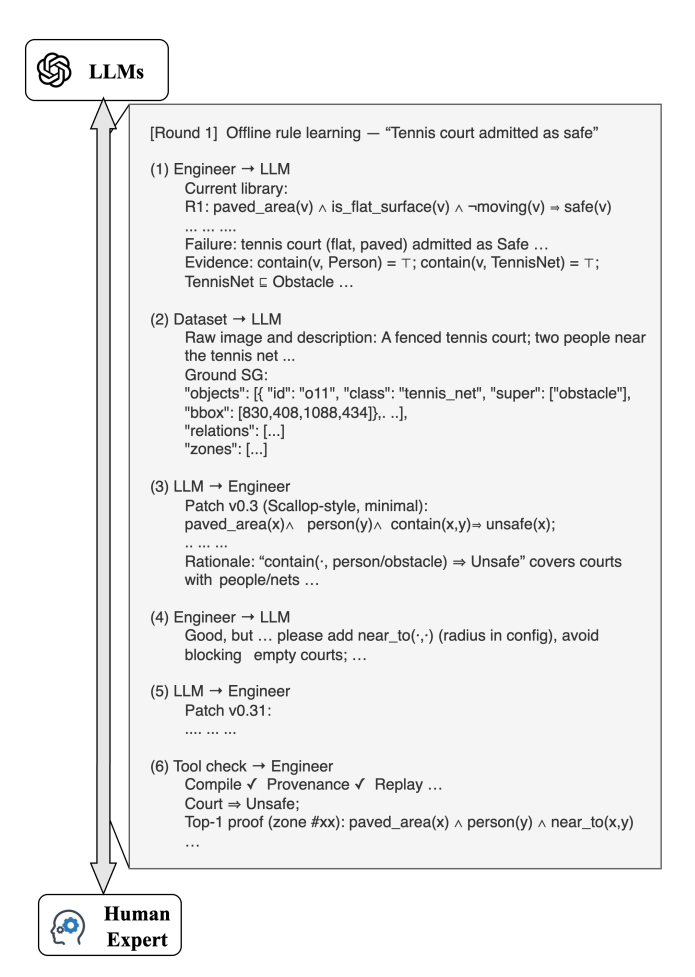


Fig. 2: Illustration of the LLM-human-in-the-loop rule learning process.

Offline training set. Our training set consists of only 72 landing site images drawn from the Semantic Drone Dataset [35]. From each image, we construct a probabilistic semantic scene graph with region attributes (class probabilities, area, slope proxies, hazard proximity, spatial relations). To enrich the prompts, we augment these graphs with (i) regional aviation regulations, (ii) domain-expert feedback from previous iterations (for correction, removal, or update of rules), and (iii) positive/negative logic rule examples. This corpus is used exclusively for rule synthesis and refinement, with no reuse in evaluation.

LLM-human synthesis loop. The LLM [15] receives the current Scallop rule library together with the prompt (scene graphs, regulations, feedback, examples) and generates candidate Scallop code (as shown in Tab. II). Human experts review the generated rules, verifying their correctness against the landing site images and providing feedback for further iterations as feedback prompt. This loop continues until the rules are consistent with both the domain knowledge and the offline training set. The verified Scallop code is then stored in a rule repository, serving as a knowledge base for the online inference stage.

Integration. At runtime, these offline-synthesized rules are compiled into probabilistic first-order logic (P-FOL) and directly executed on the online semantic scene graph built from the perception backbone. This ensures that the knowledge distilled offline is reused as an auditable, white-box safety gate during inference, enabling interpretable and verifiable SLZ decisions.

D. Online Rule Inference (Scallop)

At runtime, Scallop executes the validated rule pack as a probabilistic first-order program over the PSSG and an-

swers queries such as $\operatorname{Unsafe}(i)$ and $\operatorname{Accessible}(i)$ using $\operatorname{top-}k$ proof inference: for each region r_i , it returns the k highest-weight proofs with full provenance traces, yielding a calibrated safety score and concise, ranked explanations; regions failing the gate are pruned, and survivors are ranked by residual risk and mission context.

Fact grounding. Let $P_c^{\text{obj}}(i)$, $P_a^{\text{att}}(i)$, and $P_\rho^{\text{rel}}(i,j)$ denote calibrated confidences from the PSSG for object class c of region r_i , attribute a of r_i , and relation ρ between (r_i, r_j) , respectively. We encode each grounded fact f (e.g., PavedArea (v_i) , IsFlatSurface (v_i)) with a probability $P(f) \in [0, 1]$. For existential binary relations we pool over neighbors with a t-conorm \oplus (probabilistic sum).

$$\widehat{P}^{\mathrm{rel}}_{\rho}(i) \; = \; \bigoplus_{j \in \mathcal{N}(i)} P^{\mathrm{rel}}_{\rho}(i,j) \qquad \text{where} \;\; x \oplus y \equiv 1 - (1-x)(1-y).$$

Top-k **proofs and aggregation.** Let Π_i be the set of proofs for Unsafe(i). The weight of a proof $\pi \in \Pi_i$ is the t-norm (\otimes) product of its fact confidences (default: product t-norm $x \otimes y \equiv xy$):

$$w(\pi) = \bigotimes_{f \in facts(\pi)} P(f).$$

We approximate the overall *unsafe risk* by a noisy-OR over the *top-k* proofs,

$$R_{\text{unsafe}}(i) \approx 1 - \prod_{\pi \in \text{TopK}_k(\Pi_i)} (1 - w(\pi)),$$

 $S_{\text{safe}}(i) = 1 - R_{\text{unsafe}}(i).$

A region passes the white-box safety gate iff $S_{\rm safe}(i) \geq \tau_{\rm mission}$. Scallop's provenance semiring records which rules and facts fired (with uncertainties) in the top-k proofs, enabling auditable, human-readable justifications and robust behavior under covariate shift.

E. Multiple-Frames Validation & Mission-Specific Ranking

a) Multiple-Frames Validation (MFV).: Before scoring, we enforce temporal consistency over a short window $\mathcal{W}_T = \{t_0 - T + 1, \dots, t_0\}$ of T recent frames. A candidate zone v passes MFV if it persists and remains rule-consistent across the window. Let $v^{(t)}$ denote the tracked instance of v at time t. We define two checks: no latent hazards reappearing in any frame, and stability of geometry/pose (low jitter). Concretely,

$$\begin{aligned} \operatorname{Pass}_T(v) &\equiv \max_{t \in \mathcal{W}_T} \operatorname{hazard}\!\!\left(v^{(t)}\right) \leq \tau_{\operatorname{haz}} \; \wedge \; \operatorname{jitter}\!\!\left(v^{(\mathcal{W}_T)}\right) \leq \tau_{\operatorname{jit}}, \\ \mathbb{I}_T(v) &= \mathbf{1}\{\operatorname{Pass}_T(v)\} \in \{0,1\}. \end{aligned}$$

b) Mission-Specific Ranking (Cost-Conditioned).: After MFV, all surviving candidate landing zones are deemed safe. The final selection reduces to ranking these zones according to a mission-specific cost function that captures task preferences. For each mission m (e.g., emergency, rescue, safe-landing), we define a weighted score over normalized task-relevant features $b_{m,k}(v) \in [0,1]$ (e.g., distance to center point for emergency landing, distance to casualty for rescue, sufficient safe buffers

for safe-landing). Mission weights $\omega_{m,k} \geq 0$ encode policy priorities. The mission-conditioned score is

$$C_m(v) = \mathbb{I}_T(v) \sum_k \omega_{m,k} \, \tilde{b}_{m,k}(v), v^* = \arg\max_v C_m(v).$$

Thus, candidates failing MFV receive zero score, while passing candidates are ranked by mission-aligned utility with optional temporal aggregation for robustness.

IV. EXPERIMENTS

A. Research Questions

We investigate the following research questions (RQs) to assess NEUROSYMLAND:

- **RQ1** Effectiveness of NEUROSYMLAND. How effective is our neuro-symbolic approach when evaluated in software-in-the-loop (SIL) simulations compared with state-of-the-art UAV landing methods?
- RQ2 Efficiency analysis. How efficient is NEUROSYMLAND on edge hardware (Jetson Orin Nano Super) in terms of accuracy and computational performance under hardware-in-the-loop (HIL) evaluation?
- **RQ3** Qualitative case study. How does NEUROSYMLAND qualitatively compare with baseline methods across different landing tasks (e.g., emergency vs. rescue) in terms of safety, interpretability, and alignment with human reasoning?

To address the **RQs**, we evaluate the proposed landing-site selection framework under three complementary settings:

- Software-in-the-Loop (SIL) evaluation. Conducted in controlled simulation environments representing diverse terrain types—city streets, suburban districts, and industrial factories. Each environment is re-run under varying weather conditions (e.g., rain, snow, dust, and fog) with multiple intensity levels to assess robustness.
- Hardware-in-the-Loop (HIL) evaluation. Performed on the target edge-compute platform (Jetson Orin Nano Super) to measure stage-wise latency, computational and memory efficiency, and closed-loop control performance.
- Qualitative case studies. Comparative analyses against representative markerless baselines (e.g., VisLanding [4], SafeUAV [37]) under three mission contexts—*Emergency-Landing*, *Rescue-Landing*, and *Safe-Landing*.

B. RQ1: Effectiveness

Evaluating the *quality* of a safe landing zone (SLZ) in a *markerless* setting is intrinsically challenging and resists reduction to a single scalar value. In *marker-based* setups (e.g., AprilTag [22] or ArUco [38]), quality is typically proxied by the pose error—measured as the Euclidean distance (and sometimes yaw difference) between the predicted touchdown point and the tag center. Lacking such an external reference, we assess the *quality of successful SLZs* using two interpretable and complementary metrics. Throughout, let $\hat{\mathbf{p}} \in \mathbb{R}^2$ denote the predicted touchdown point, \mathcal{O} the set of obstacle boundary points (e.g., fences, building edges, pool rims, trees),

c the centroid of the image (drone position), and $\|\cdot\|_2$ the Euclidean norm.

1) Minimum Obstacle Distance (MOD†):

$$\mathrm{MOD} \; = \; \min_{\mathbf{o} \in \mathcal{O}} \left\| \hat{\mathbf{p}} - \mathbf{o} \right\|_2,$$

where a larger value indicates a safer buffer zone and higher tolerance to localization errors.

2) Touchdown-Centroid Distance (TCD↓):

$$TCD = \|\hat{\mathbf{p}} - c\|_2,$$

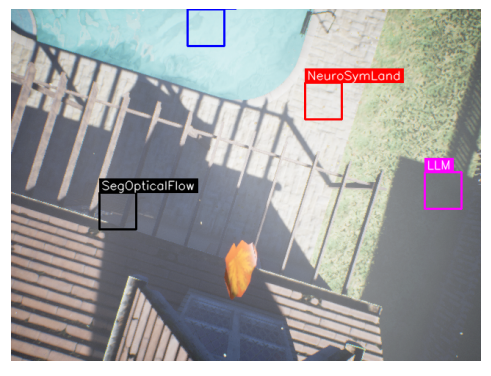
where a smaller value implies reduced lateral maneuvering and consequently lower operational risk.

- a) Experiment Setup.: We conduct evaluations in Air-Sim [39] using 15 distinct maps that represent common UAV operating environments, including city streets, suburban areas, industrial yards, parking lots, parks/grass fields, and construction sites. From each map, we preselect two candidate landing zones (yielding a total of 30 SLZs) and re-run the same candidates under multiple weather conditions—clear, rain, snow, fog, and dust—each at light, medium, and heavy intensity levels. To increase environmental variability, we further randomize the wind vector and time of day (dawn, noon, dusk) for each trial.
- b) Baseline.: We do not directly benchmark against prior markerless landing pipelines [40], [4], [2] that rely on heavier sensing modalities (e.g., depth cameras or LiDAR) or full SLAM stacks executed on laptop- or desktop-class hardware, as such comparisons would introduce confounding factors due to unequal sensing and computational capabilities. Instead, we implement lightweight counterparts inspired by well-established approaches [41], [42], [43], [44], [45], ensuring fair, controlled evaluation on the same set of candidate SLZs and under identical Jetson-class computational budgets. This design choice isolates algorithmic differences from hardware or sensor advantages, allowing a more principled comparison of reasoning quality and efficiency.
 - SegOpticalFlow [41], [42]: a perception-only baseline that evaluates candidate sites using multi-frame optical flow estimates; it employs the same perception backbone as NEUROSYMLAND.
 - **DetFOL** [43], [44]: a deterministic first-order logic (FOL) variant constructed over the identical rule set, sharing the same perception backbone. Unlike NEUROSYM-LAND, which synthesizes executable SCALLOP programs through an offline neuro-symbolic pipeline, DetFOL encodes the same reasoning as hand-crafted FOL predicates evaluated deterministically at runtime. This design isolates the benefit of neuro-symbolic synthesis—learning rule weights and probabilistic bindings—from the underlying logical structure itself.
 - LLM-Explain: a local vision—language model (VLM) [45] prompted with the scene image and encoded safety rules; it selects among the same candidate sites and provides a concise textual rationale. This baseline reflects the growing industry inclination to adopt VLMs

as direct decision-makers for perception-driven tasks due to their strong visual-semantic reasoning capabilities. Our comparison aims to examine whether such end-to-end reasoning remains reliable when subjected to mission-critical constraints—and to what extent a neuro-symbolic framework with explicit logical guardrails can improve decision consistency and safety compliance.

TABLE III: Quality on successful SLZs in the AirSim test set.

Model	MOD↑	TCD↓
NEUROSYMLAND (ours)	112.81	126.77
SegOpticalFlow	96.13	162.36
DetFOL	73.46	208.30
LLM-Explain	61.86	238.88



(a) Good case.



(b) Failure case.

Fig. 3: **Qualitative outcomes in the Airsim.** Two representative cases illustrate how the pipeline behaves under different scene conditions.

c) Result Analysis:: The experiment shows NEUROSYM-LAND is Pareto-superior on both safety buffer (MOD↑) and maneuver economy (TCD↓). Compared to SegOpticalFlow, it yields a +17.4% increase in MOD (112.81 vs. 96.13) and a 21.9% reduction in TCD (126.77 vs. 162.36), indicating both wider hazard stand-off and less lateral adjustment prior to commit. Against DetFOL (same rules/backbone but deterministic), gains are larger: +53.6% MOD (112.81 vs. 73.46) and 39.1% lower TCD (126.77 vs. 208.30), suggesting that probabilistic reasoning improves ranking among feasible

candidates. The gap is greatest versus LLM-Explain (+82.4% MOD; 46.9% lower TCD), reflecting that natural-language rationales without structured inference underperform on precise buffer and placement criteria. Overall, NEUROSYMLAND consistently selects landing sites that are farther from obstacles while closer to region centroids, aligning with the monotonic objectives MOD↑ and TCD↓ used for quality evaluation.

d) Case studies:: Fig. 3 summarizes two representative scenes that highlight both strengths and current limitations.

Good case (Fig. 3a). In a residential backyard with a swimming pool and a nearby fence line, NEUROSYMLAND correctly selects a landing site next to the pool on open ground, maintaining a safe standoff from water and structural edges. In contrast, (i) DetFOL places the site on the pool surface (unsafe), (ii) SegOpticalFlow selects the narrow edge along the house (insufficient clearance), and (iii) LLM-Explain locks onto the fence's shadow region close to the fence (unsafe). The success of NEUROSYMLAND stems from explicit symbolic rules that penalize proximity to water bodies and rigid obstacles, combined with spatial margins that down-weight thin or borderline regions prone to optical or shading artifacts.

Failure case (Fig. 3b). In a rooftop scene, all methods (NEUROSYMLAND, LLM-Explain, DetFOL, SegOpticalFlow) predict landing sites on the roof. The shared failure arises from upstream perception: the backbone segmentation model misclassifies roof surfaces as flat ground, causing all downstream selectors to inherit this bias. This represents a discriminative failure of the foundation vision model rather than an error in the symbolic reasoning layer. Although our rules explicitly forbid landing on roofs, they can only operate correctly when the perception stage provides faithful semantic labels. Improving robustness thus requires enhancing perception fidelity-e.g., expanding training data to better distinguish roofs from ground, incorporating multi-view or depth consistency checks, or adding geometric cues such as slope and height thresholds. Overall, the qualitative outcomes (Fig. 3) align with the aggregate trends (Tab. III): the proposed pipeline effectively avoids water, fence, and edge hazards in complex yard scenes, yet remains sensitive to systematic mislabeling by the segmentation backbone. This limitation points to future work on deeper neuro-symbolic binding within the latent space of VLM/LLM components—ensuring that core physical and semantic concepts such as roof, ground, and flat terrain are properly disentangled and symbolically aligned. Strengthening this conceptual alignment, rather than relying solely on training data which may never be perfect and enough, may lead to more consistent high-level reasoning and safer landing decisions.

C. RQ2: Efficiency

To quantify end-to-end responsiveness and closed-loop robustness of NEUROSYMLAND on target hardware under realistic I/O, we use the same candidate SLZ set as in simulation for a controlled comparison.

a) Setup:: The hardware platform for all hardware-in-the-loop (HIL) evaluations is a Jetson Orin Nano Su-

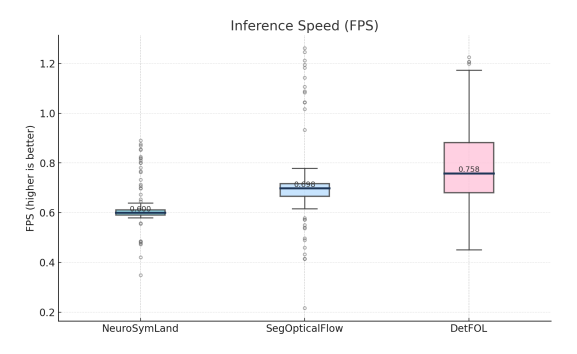


Fig. 4: Inference speed (FPS; higher is better). Boxes show the median and IQR; whiskers denote $1.5 \times IQR$; dots are outliers. FPS is computed from per-trial latency (FPS = 1000/ms) under identical hardware and settings.

TABLE IV: Stage-wise latency (ms) of NEUROSYMLAND.

Model	Percep.	Post proc.	PSSG	Symbolic
NEUROSYMLAND (ours)	312	350	997	8

per equipped with 8 GB RAM, running Ubuntu 22.04 with CUDA 12.6 and ONNX Runtime 1.19. The perception stack employs *SegFormer-B0-INT8* for semantic segmentation. The control loop integrates the *PX4 Autopilot* through the *MAVROS/ROS 2 Humble* bridge at a 30 Hz update rate, and all simulations are conducted in *AirSim* [39].

For each environment–weather–intensity configuration, we execute 100 trials with randomized initial poses and headings randomly selected from one of the simulation maps described earlier. During each run, we log stage-wise timestamps (segmentation perception \rightarrow post-processing \rightarrow PSSG construction \rightarrow symbolic reasoning) as well as system utilization metrics, including CPU/GPU usage, memory consumption, power, and temperature. To contextualize efficiency, we compare Neurosymland against two lightweight baselines that are directly compatible with the same deployment stack: SegOpticalFlow and DetFOL.

b) Results Analysis:: Figure 4 compares the inference speed of NEUROSYMLAND, SegOpticalFlow, and DetFOL under identical hardware and configuration settings. NEUROSYMLAND achieves a median throughput of 0.600 FPS (IQR 0.021), corresponding to 1,668 ms per frame; SegOpticalFlow and DetFOL attain 0.698 FPS (IQR 0.050, 1,433 ms) and 0.758 FPS (IQR 0.202, 1,319 ms), respectively. Although NEUROSYMLAND runs slightly slower in median FPS, it remains practically deployable on the edge drone platform for the landing task, where a refresh rate of 0.5–1 s per frame is acceptable for safe decision making.

For fair comparison, inference speed is evaluated across all baselines; however, stage-wise latency analysis is reported only for NeurosymLand, as this decomposition is unique to its neuro-symbolic pipeline and provides diagnostic insight into internal computational efficiency. Understanding which components dominate end-to-end latency is crucial for targeted

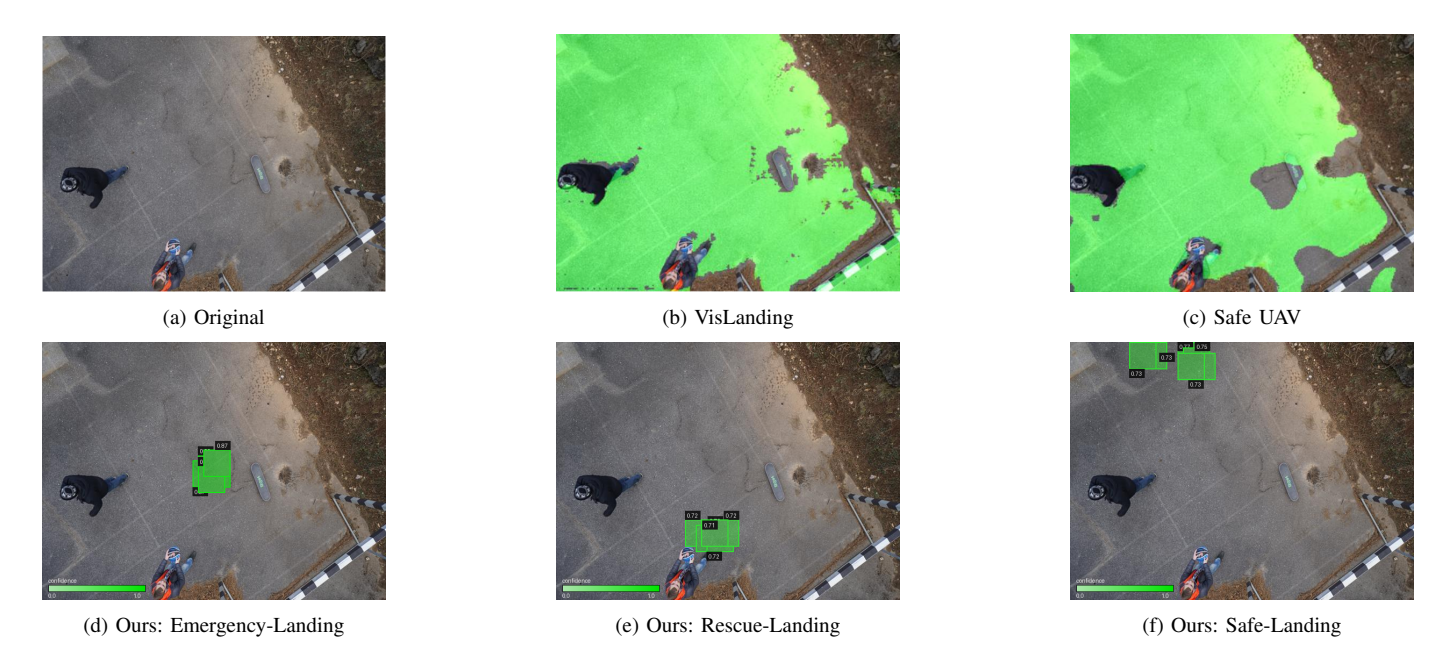


Fig. 5: Case study for a skateboard park. Green: feasible SLZ. Only the top-k candidates (k = 10) are shown in ours to avoid clutter; inference uses the full candidate set.

TABLE V: System metrics on Jetson Orin.

Model				Power (W)	
NEUROSYMLAND (ours)	76.87	33	3.28	1.23	47.91
DetFOL	77.12	33	3.10	1.196	47.21
SegOpticalFlow	59.82	33	2.09	1.07	45.20

optimization. As shown in Table IV, the main bottleneck arises from PSSG construction (997 ms, $\sim 60\%$ of total latency), followed by post-processing (350 ms, $\sim 21\%$) and perception (312 ms, $\sim 19\%$), while symbolic reasoning contributes negligibly (8 ms, < 1%).

System-level performance metrics, summarized in Table V, are collected for all methods under identical deployment conditions on the Jetson Orin Nano. NEUROSYMLAND exhibits moderate utilization (CPU 76%, GPU 33%, memory 3.3 GB, power 1.23 W, temperature 48°C), indicating substantial headroom for additional onboard tasks. For comparison, SegOpticalFlow shows [CPU 59.8%/ GPU 33% / memory 2.09 GB / power 1.07 W / temperature 45°], and DetFOL records [CPU 77%/ GPU 33% / memory 3.28 GB / power 1.19 W / temperature 47.2°]. Overall, despite being marginally equivalent compared with these lightweight baselines, NEUROSYMLAND 's throughput and efficiency remain well within the constraints of edge deployment, and its reasoning layer introduces virtually no additional overhead.

D. RQ3: Qualitative Study.

a) Setup:: Both VisLanding [4] and SafeUAV [37] are safety-oriented, markerless landing pipelines designed to locate safe landing zones based purely on geometric and obstacle constraints. They do not incorporate mission-specific ranking



Fig. 6: **Semantic node distribution (Ours).** Calibrated segmentation is overlaid on the RGB frame; colors indicate classes (e.g., paved, vegetation, person, obstacle). The white grid is the spatial index used for candidate sampling, with zone IDs shown at centers.

heuristics—such as assigning higher priority to proximity-based objectives like "closer to the center" for emergency touchdowns or "closer to a rescue target" for search-andrescue operations. To ensure a fair comparison, since these methods operate only at the image level—unlike our approach, which processes multiple frames and can be executed in simulation—we evaluate them *as-is* on randomly selected landing site images drawn from the same dataset used by our method.

In contrast, NEUROSYMLAND introduces a mission-specific ranking mechanism that dynamically adjusts the weights of symbolic predicates to capture task-dependent priorities—for

TABLE VI: Rule-level contributions (Scallop provenance) for case study, zone #65.

Rule r_*	p	#proofs
r_hazard_near_person	0.888313	1
r_hazard_near_obstacle	0.777675	1
r_hazard_adj_pool	0.000000	0
r_hazard_near_tree	0.000000	0
r_hazard_cont_car	0.000000	0
r_hazard_cont_person	0.000000	0
r_hazard_cont_obsL	0.000000	0
r_hazard_cont_vegL	0.000000	0

Notes. Values are extracted from Scallop's provenance

(difftopkproofsdebug); a rule's proof weight is the semiring product of its supporting facts. This table exposes *which* safety rules drive the final hazard judgment for the chosen SLZ.

example, assigning greater importance to the *distance-to-center* predicate during emergency landings. To evaluate the effect of these mission-conditioned weightings, we compare the landing performance of NEUROSYMLAND against VisLanding and SafeUAV across three mission contexts that differ only in their *weighted cost functions*, all applied to the same candidate SLZ set:

- Emergency: prioritizes minimal distance to a predefined mission center, favoring rapid and nearby touchdowns.
- Rescue: prioritizes minimal distance to a target waypoint or person of interest, emphasizing proximity to the rescue objective.
- Safe-Landing: prioritizes larger safety margins by assigning higher cost to proximity with hazards (e.g., roads, buildings, water, crowds) and to poor surface conditions (e.g., slope, roughness), thereby encouraging conservative touchdown zones.

For each scene, we present the *original image*, the *VisLanding* output, and the mission-specific outputs of NEUROSYM-LAND (*Emergency*, *Rescue*, and *Safe-Landing*). All methods operate on identical inputs; NEUROSYMLAND differs only in its mission-specific cost weighting, which adapts the same symbolic reasoning process to different operational objectives.

b) Results:: From Fig. 5, both VisLanding (Fig. 5b) and SafeUAV (Fig. 5c) tend to label large paved areas as globally "safe," prioritizing geometric feasibility while providing limited consideration of buffer space to nearby hazards (e.g., pedestrians, small obstacles, curb edges). In contrast, NEUROSYMLAND in the Safe-Landing setting explicitly penalizes small safety margins: candidates with larger clearance (high MOD*) and greater stand-off from hazards are ranked higher, resulting in touchdown choices that are visibly farther from people and clutter. Under Emergency-Landing, the symbolic mission-specific cost function emphasizes proximity to the mission center while maintaining adequate clearance—NEUROSYMLAND selects a zone near the center that still preserves a safe buffer from pedestrians. Under **Rescue-Landing**, the symbolic mission-specific cost function prioritizes proximity to the target waypoint or person; NEUROSYMLAND selects a zone adjacent to, but not overlapping with, the person's footprint, thereby respecting

the non-intersection constraint while maintaining a workable safety buffer.

c) Case study.: In contrast to deep end-to-end baselines that operate as black boxes, our selector produces a proofcarrying decision. Figure 6 illustrates the calibrated segmentation overlaid with our evaluation grid, where zone #65 lies on a paved surface. From Scallop's provenance trace (Tab. VI), two rules activate with high weights: r hazard near person (p = 0.888) and r_hazard_near_obstacle (p = 0.778), while all pool-, tree-, and container-related rules contribute negligibly (p = 0). The top-level proofs are explicit: paved_area(65) \otimes person(89) \otimes near_to(65, 89) and paved area $(65) \otimes \text{obstacle}(95) \otimes \text{near to}(65, 95)$. This rulelevel attribution renders the rationale transparent: safety engineers can (i) formally verify whether the SLZ satisfies—or violates-explicit preconditions (e.g., human or obstacle standoff), (ii) trace and replay the corresponding proof during certification or regression testing, and (iii) customize policy behavior by editing rule thresholds (e.g., the radius parameter in near to) without retraining any neural network. By contrast, black-box testing provides only dataset-level performance metrics (e.g., AP or F1), offering no property-level guarantees, limited robustness to distribution shifts, and weak requirements traceability.

V. CONCLUSION AND FUTURE WORK

This paper presented NEUROSYMLAND, a neuro-symbolic framework for UAV safe-landing-zone detection that combines human-in-the-loop rule synthesis with Scallop-based probabilistic first-order logic. Unlike conventional black-box models, NEUROSYMLAND decouples perception from symbolic safety logic, synthesizes interpretable rules offline, and executes them online as verifiable white-box safety gates over lightweight scene graphs. Across both simulation and hardware-in-the-loop evaluations, NEUROSYMLAND achieves higher reliability and transparency while demonstrating strong interpretability, verifiability, and testability—marking a step toward certifiable AI-driven safety.

Future work will advance this foundation along three key directions. First, temporal reasoning: extending the preprocessing pipeline across multiple frames to construct lightweight temporal—spatial scene graphs that encode dynamic relations (e.g., "getting closer", "moving away") for richer safety semantics. Second, concept alignment in foundation models: refining UAV-landing-related latent representations within VLM/LLM backbones to ensure critical concept consistency (e.g., roof vs. ground, flat vs. sloped surfaces). Third, multimodal neuro-symbolic fusion: integrating and symbolically reasoning over diverse sensors (LiDAR, radar, thermal, stereo) to characterize their respective advantages and limitations across landing contexts, enabling logical and interpretable sensor fusion under resource constraints.

REFERENCES

[1] T. Hinzmann, T. Stastny, C. Cadena, R. Siegwart, and I. Gilitschenski, "Free lsd: Prior-free visual landing site detection for autonomous

- planes," *IEEE Robotics and Automation Letters*, vol. 3, no. 3, pp. 2545–2552, 2018.
- [2] P. Schoppmann, P. F. Proença et al., "Multi-resolution elevation mapping and safe landing site detection with applications to planetary rotorcraft," 2021. [Online]. Available: https://arxiv.org/abs/2111.06271
- [3] M. Secchiero, N. Bobbili, Y. Zhou, and G. Loianno, "Visual environment assessment for safe autonomous quadrotor landing," 2024. [Online]. Available: https://arxiv.org/abs/2311.10065
- [4] Z. Tan, B. He, Y. Ji, and L. Wu, "Vislanding: Monocular 3d perception for uav safe landing via depth-normal synergy," 2025. [Online]. Available: https://arxiv.org/abs/2506.14525
- [5] G. Loureiro, A. Dias, A. Martins, and J. Almeida, "Emergency landing spot detection algorithm for unmanned aerial vehicles," *Remote Sensing*, vol. 13, no. 10, p. 1930, 2021.
- [6] J. Chen, W. Du et al., "Emergency uav landing on unknown field using depth-enhanced graph structure," T-ASE, 2024.
- [7] S. H. Alsamhi, A. V. Shvetsov et al., "Uav computing-assisted search and rescue mission framework for disaster and harsh environment mitigation," *Drones*, vol. 6, no. 7, p. 154, 2022.
- [8] C. Dahal, H. B. Dura, and L. Poudel, "Design and analysis of propeller for high-altitude search and rescue unmanned aerial vehicle," *Interna*tional Journal of Aerospace Engineering, vol. 2021, no. 1, p. 6629489, 2021
- [9] Y. Lun, H. Wang et al., "Target search in dynamic environments with multiple solar-powered uavs," TVT, vol. 71, no. 9, pp. 9309–9321, 2022.
- [10] F. Betti Sorbelli, "Uav-based delivery systems: A systematic review, current trends, and research challenges," *Journal on Autonomous Trans*portation Systems, vol. 1, no. 3, pp. 1–40, 2024.
- [11] X. Li, J. Tupayachi, A. Sharmin, and M. Martinez Ferguson, "Drone-aided delivery methods, challenge, and the future: A methodological review," *Drones*, vol. 7, no. 3, p. 191, 2023.
- [12] D. Dissanayaka, T. R. Wanasinghe, O. De Silva, A. Jayasiri, and G. K. Mann, "Review of navigation methods for uav-based parcel delivery," *IEEE Transactions on Automation Science and Engineering*, vol. 21, no. 1, pp. 1068–1082, 2023.
- [13] E. Kakaletsis, C. Symeonidis et al., "Computer vision for autonomous uav flight safety: An overview and a vision-based safe landing pipeline example," Acm Computing Surveys (Csur), vol. 54, no. 9, pp. 1–37, 2021.
- [14] C. Rudin, "Stop explaining black box machine learning models for high stakes decisions and use interpretable models instead," *Nature Machine Intelligence*, vol. 1, no. 5, pp. 206–215, 2019.
- [15] OpenAI, "Chatgpt: O3-mini," https://openai.com/chatgpt, 2025, large language model.
- [16] G. Katz, C. Barrett, D. L. Dill, K. Julian, and M. J. Kochenderfer, "Reluplex: An efficient SMT solver for verifying deep neural networks," in *Computer Aided Verification (CAV 2017)*, ser. Lecture Notes in Computer Science, vol. 10426. Springer, 2017, pp. 97–117.
- [17] G. Katz, D. A. Huang et al., "The marabou framework for verification and analysis of deep neural networks," in Computer Aided Verification (CAV 2019), ser. Lecture Notes in Computer Science, vol. 11561. Springer, 2019, pp. 443–452.
- [18] Z. Li, J. Huang, and M. Naik, "Scallop: A language for neurosymbolic programming," *Proceedings of the ACM on Programming Languages*, vol. 7, no. PLDI, Jun 2023.
- [19] A. d'Avila Garcez and L. C. Lamb, "Neurosymbolic ai: The 3rd wave," 2020. [Online]. Available: https://arxiv.org/abs/2012.05876
- [20] E. Marconato, G. Bontempo, E. Ficarra, S. Calderara, A. Passerini, and S. Teso, "Neuro-symbolic continual learning: Knowledge, reasoning shortcuts and concept rehearsal," 2023. [Online]. Available: https://arxiv.org/abs/2302.01242
- [21] G. I. Parisi, R. Kemker, J. L. Part, C. Kanan, and S. Wermter, "Continual lifelong learning with neural networks: A review," *Neural Networks*, vol. 113, pp. 54–71, 2019.
- [22] E. Olson, "Apriltag: A robust and flexible visual fiducial system," in 2011 IEEE International Conference on Robotics and Automation (ICRA). IEEE, 2011, pp. 3400–3407.
- [23] J. Wang and E. Olson, "Apriltag 2: Efficient and robust fiducial detection," in 2016 IEEE/RSJ International Conference on Intelligent Robots and Systems (IROS), Daejeon, South Korea, 2016.
- [24] S. Garrido-Jurado, R. Muñoz-Salinas, F. J. Madrid-Cuevas, and M. J. Marín-Jiménez, "Automatic generation and detection of highly reliable fiducial markers under occlusion," *Pattern Recognition*, vol. 47, no. 6, pp. 2280–2292, 2014.

- [25] J. W. Lloyd, Foundations of Logic Programming, 2nd ed. Berlin, Heidelberg: Springer, 1987.
- [26] L. De Raedt, A. Kimmig, and H. Toivonen, "Problog: A probabilistic prolog and its application in link discovery," in *IJCAI*, Hyderabad, India, 2007, pp. 2462–2467.
- [27] R. Manhaeve, S. Dumančić, A. Kimmig, T. Demeester, and L. De Raedt, "Deepproblog: Neural probabilistic logic programming," in Advances in Neural Information Processing Systems (NeurIPS), 2018.
- [28] W. W. Cohen, "Tensorlog: A differentiable deductive database," arXiv preprint arXiv:1605.06523, 2016. [Online]. Available: https://arxiv.org/abs/1605.06523
- [29] J. Huang, Z. Li et al., "Scallop: From probabilistic deductive databases to scalable differentiable reasoning," in Advances in Neural Information Processing Systems (NeurIPS 2021), 2021.
- [30] M. Ahn, A. Brohan et al., "Do as i can, not as i say: Grounding language in robotic affordances," 2022. [Online]. Available: https://arxiv.org/abs/2204.01691
- [31] J. Liang, W. Huang *et al.*, "Code as policies: Language model programs for embodied control," 2023. [Online]. Available: https://arxiv.org/abs/2209.07753
- [32] L. Gao, A. Madaan, S. Zhou, U. Alon, P. Liu, Y. Yang, J. Callan, and G. Neubig, "Pal: Program-aided language models," 2023. [Online]. Available: https://arxiv.org/abs/2211.10435
- [33] X. Ye, Q. Chen, I. Dillig, and G. Durrett, "Satlm: Satisfiability-aided language models using declarative prompting," 2023. [Online]. Available: https://arxiv.org/abs/2305.09656
- [34] E. Xie, W. Wang, Z. Yu, A. Anandkumar, J. M. Alvarez, and P. Luo, "Segformer: Simple and efficient design for semantic segmentation with transformers," 2021. [Online]. Available: https://arxiv.org/abs/2105.15203
- [35] I. of Engineering Geodesy and G. U. o. T. Measurement Systems (IGMS), "Semantic drone dataset," https://www.tugraz.at/index.php?id=22387.
- [36] G. Bradski, "The OpenCV Library," Dr. Dobb's Journal of Software Tools, 2000.
- [37] A. Marcu, D. Costea, V. Licaret, M. Pîrvu, E. Slusanschi, and M. Leordeanu, "Safeuav: Learning to estimate depth and safe landing areas for uavs from synthetic data," in *ECCV Workshops*, 2018, pp. 0–0.
- [38] I. Lebedev, A. Erashov, and A. Shabanova, "Accurate autonomous uav landing using vision-based detection of aruco-marker," in *Interac*tive Collaborative Robotics, ser. Lecture Notes in Computer Science. Springer, 2020, vol. 12336, pp. 179–188.
- [39] S. Shah, D. Dey, C. Lovett, and A. Kapoor, "Airsim: High-fidelity visual and physical simulation for autonomous vehicles," in *Field and Service Robotics: Results of the 11th International Conference*. Springer, 2018, pp. 621–635.
- [40] M. Mittal, R. Mohan, W. Burgard, and A. Valada, "Vision-based autonomous uav navigation and landing for urban search and rescue," in *The International Symposium of Robotics Research*. Springer, 2019, pp. 575–592.
- [41] H. W. Ho, G. C. H. E. de Croon, E. van Kampen, Q. P. Chu, and M. Mulder, "Adaptive gain control strategy for constant optical flow divergence landing," *IEEE Transactions on Robotics*, vol. 34, no. 2, pp. 508–516, 2018
- [42] K. Y. W. Scheper and G. C. H. E. de Croon, "Evolution of robust high-speed optical-flow-based landing for autonomous micro air vehicles," *Robotics and Autonomous Systems*, vol. 124, p. 103380, 2020.
- [43] A. E. Johnson, J. F. Montgomery, and L. H. Matthies, "Vision-guided landing of an autonomous helicopter in hazardous terrain," in *Proceedings of the IEEE International Conference on Robotics and Automation* (ICRA), 2005, pp. 3966–3971.
- [44] S. Saripalli, J. F. Montgomery, and G. S. Sukhatme, "Visually-guided landing of an unmanned aerial vehicle," *IEEE Transactions on Robotics* and Automation, vol. 19, no. 3, pp. 371–380, 2003.
- [45] M. Abdin et al., "Phi-3 technical report: A highly capable language model locally on your phone," 2024. [Online]. Available: https://arxiv.org/abs/2404.14219